Breaking the temperature barrier

Unveiling the potential of ceria nanorods for low temperature thermochemical water splitting

R.Naikwadi, Dhanaji; Ganesh, Vaishnavi; Sharaf, Hesham; Offidani, Michele; Albonetti, Stefania; Dimitratos, Nikolaos; Bansode, Atul

DOI
10.1016/j.fuel.2025.135251

Publication date
2025

Document Version
Final published version

Published in
Fuel

Fuel 397 (2025) 135251

Contents lists available at ScienceDirect

Fuel

journal homepage: www.elsevier.com/locate/fuel

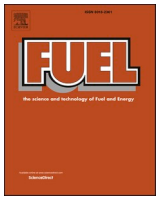

Short communication

Breaking the temperature barrier: Unveiling the potential of ceria nanorods for low temperature thermochemical water splitting

Dhanaji R.Naikwadi [a,1], Vaishnavi Ganesh [a,1], Hesham Sharaf [a], Michele Offidani [b,c], Stefania Albonetti [b,c], Nikolaos Dimitratos [b,c], Atul Bansode [a,*]

[a] Department of Chemical Engineering, Delft University of Technology, Van der Massweg 9, 2629 HZ Delft, the Netherlands
[b] Department of Industrial Chemistry "Toso Montanari", University of Bologna, Viale Risorgimento 4, 40136 Bologna, Italy
[c] Center for Chemical Catalysis—C3, Alma Mater Studiorum Università di Bologna, Viale Risorgimento 4, 40136 Bologna, Italy

ARTICLE INFO

Keywords:
Ceria nanorods
Oxygen vacancy
Isothermal
Thermochemical water-splitting
Hydrogen

ABSTRACT

Thermochemical Water-Splitting (TCWS) is a promising approach for generating clean hydrogen (H_2) by employing the waste heat originating from different sources. High-temperature requirements and temperature swing approach hinder the widespread adoption of TCWS for clean hydrogen production. This study explores ceria nanorods (CeNRs) as a potential solution for overcoming these limitations. Herein, we report, the TCWS in a fixed bed reactor using CeNRs at low and constant temperature of 400 °C. We systematically explore the influence of synthesis parameters on the resulting CeNRs, including the selection of ceria precursor, effect of calcination, and their impact in TCWS. It was found that CeNRs prepared using cerium chloride as the precursor exhibited enhanced TCWS activity, resulting significantly higher total H_2 yield 4.74 mL/g, at a constant temperature of 400 °C in three redox cycles. Moreover, X-ray Photoelectron Spectroscopy (XPS) analysis confirms the presence of both Ce^{3+} and Ce^{4+} states within the structure, with Ce^{3+} constituting approximately 30 % and Ce^{4+} accounting for approximately 70 % of the total cerium content. Additionally, Raman spectroscopy corroborates the presence of a higher concentration of oxygen vacancy which are beneficial for increasing the hydrogen production. We demonstrate that ceria in its nanorod structure having exposed higher proportions of (110) and (100) planes and higher concentration of oxygen vacancies is beneficial for lowering TCWS temperature as well as increasing the hydrogen yield.

1. Introduction

Driven by escalating climate change concerns and the depletion of finite fossil fuel reserves, the demand for clean and sustainable energy alternatives is rapidly increasing. Hydrogen, a renewable and carbon-free energy carrier, has emerged as a frontrunner in this pursuit due to its versatility and environmental benefits [1]. Projections indicate that the demand for clean hydrogen from low-carbon sources could reach 519.1 million metric tonnes annually by 2070, [2–4] a significant increase from 71 million tonnes in 2019. Unlike the previous focus on hydrogen for fuel cells in transport, current discussions encompass a broad range of possibilities for hydrogen use, gaining political support globally. Hydrogen is now a key element in mainstream energy conversations, with countries and companies recognizing its potential as a valuable component of the future energy system [1–6].

Although hydrogen is often proposed as a sustainable alternative, this largely depends on the method with which the hydrogen is produced, depending on its source [6]. Among the available green technologies for hydrogen production, water splitting is considered one of the most environmentally friendly methods for replacing fossil fuels [6,7]. Over the past few decades, numerous efforts have been devoted to develop more efficient and sustainable methods for hydrogen production through water splitting reactions including electrolysis, photolysis, and combined photoelectrochemical water splitting [8]. Despite the advancements in renewable hydrogen production methods, a vast majority (95 %) of hydrogen still comes from non-renewable sources, and water splitting only contributes to 3.9 % of the total hydrogen production [8]. To meet the rising demand for green hydrogen, it is essential to explore all possible pathways for hydrogen generation from water using renewable energy sources, ensuring a sustainable and efficient future

* Corresponding author.
E-mail address: a.b.bansode@tudelft.nl (A. Bansode).
[1] Equal contribution

https://doi.org/10.1016/j.fuel.2025.135251
Received 11 December 2024; Received in revised form 15 March 2025; Accepted 29 March 2025

[9]. TCWS is an attractive way of using thermal energy for hydrogen generation, either from solar radiation or renewable electricity in remote locations [9]. It offers the potential for high efficiency and scalability as it can be integrated with existing thermal processes for the utilisation of waste heat to provide a steady and reliable hydrogen supply [10]. A key challenge that has slowed its commercialisation and widespread adoption is the high temperature requirement that imposes a high cost on this technology. Conventional TCWS systems employing redox materials, mainly using Ceria (CeO_2) by virtue of its high oxygen storage capacity and redox activity, require high reduction temperatures (>1200 °C) and proceed via a two-step temperature swing mechanism [9–12]. According to literature reports, (Supporting information, Table S1) high temperatures exceeding in the range of 900 °C to 1500 °C are required for water splitting, which proceeds through a two-step temperature swing mechanism. This mechanism typically involves the thermal reduction of a metal oxide at high temperature, followed by reoxidation with water at a lower temperature to produce hydrogen. This poses another challenge of thermal stress on the redox material and loss of process efficiency from the irreversible heat losses due to the cooling and reheating during multiple redox cycles [13–20].

Cerium dioxide is a notable material in catalysis due to its redox behaviour (Ce^{3+}/Ce^{4+}). Studies suggest that the shape of ceria nanostructures plays a significant role in their catalytic behaviour, with rod-shaped morphologies offering advantages over other shapes [21–40]. Ceria possesses a unique crystal structure (fluorite lattice) that allows for non-stoichiometry, leading to the formation of oxygen vacancies within its structure. This inherent defect chemistry, often attributed to the larger ionic radius of Ce^{3+} compared to Ce^{4+}, contributes to ceria's exceptional redox properties. Interestingly, CeNRs structure exhibit a higher concentration of oxygen vacancies (Ce^{3+}/Ce^{4+} ratio) compared to other nanostructures due to their preferential exposure of reactive crystal planes {1 1 0} and {1 0 0}. CeNPs stands for ceria nanoparticles, which are nano-sized spherical particles of CeO_2. Typical CeNPs, on the other hand, are dominated by less reactive {1 1 1} planes [11]. Unlike nanoparticles with polyhedral structures exposing eight {1 1 1} or a combination of eight {1 1 1} and six {1 0 0} planes, rod-shaped nanostructures preferentially expose four {1 1 0} and two {1 0 0} planes [10–16]. This characteristic enhances oxygen exchange capability, a crucial factor for catalytic reactions like CO oxidation, oxidative/non-oxidative coupling and other organic reactions and more importantly a key factor in thermal water splitting reaction that is based on redox cycles [11–22]. Having higher oxygen storage capacity is beneficial for TCWS to enhance the hydrogen yield [40–56]. CeNRs allow oxygen species on both the surface and in the bulk to participate in the redox cycle, resulting in a higher oxygen storage capacity (Ce^{3+}/Ce^{4+}). The oxygen storage capacity (related to exposed crystal planes) of ceria follows the order of: nanocubes > nanorods > nanopolyhedra, indicating that low-indexed planes exhibit higher oxygen storage capacity [23]. CeO_2-MOx solid solutions exhibited higher H_2 production than pure ceria at reduction temperatures above 1400 °C. CeO_2-NiO produced the most H_2 (1.446 ml/g) at 1400 °C, while CeO_2-MnO reached 3.773 ml/g at 1500 °C. Among them, CeO_2-Fe_2O_3 was the most stable over multiple cycles, maintaining consistent O_2 release (1.33 ml/g at 1400 °C) and H_2 production (2.26 ml/g at 1000 °C). Kaneko et al. studied H_2O splitting using ceria in a rotary solar reactor, with a maximum reduction temperature of 1350 °C. At this temperature, ceria released negligible O_2, and its re-oxidation at 1000 °C produced 0.68 ml/g of H_2, lower than the 0.76 ml/g obtained at 1500 °C [56–61].

Driven by the enhanced redox properties of CeNRs and their potential for a higher concentration of oxygen vacancies [24–35], we report the application of CeNR structures in TCWS to reduce the overall reaction temperature. This research effort paves the way for developing CeNRs as efficient and robust redox material for low-temperature TCWS-based hydrogen generation.

2. Result and discussion

The CeNRs were synthesized by using two different ceria precursors. (Detailed procedure explained in supporting information page no S2). The type of ceria precursor also has an influence on morphology of CeNRs [22]. Typically, the formation of nanorods proceeds via the reaction of ceria precursor with hydroxides (HO^-) in a basic solution (NaOH) to form $Ce(OH)_3$ (cerium hydroxide, Ce^{3+}). The formation of $Ce(OH)_3$ involves an additional nucleation step, which is crucial for controlled anisotropic crystal growth. Importantly, the counter ions in the solution (such as Cl^- and NO_3^-) are vital for the controlled growth of $Ce(OH)_3$. Wu et al. examined the effect of anions like Cl^-, Br^-, and I^- on the formation nanorods [29]. It was mentioned that during nucleation and crystal growth, halides partially adsorb on the surface of $Ce(OH)_3$, stabilizing it and promoting the formation of CeNRs with some Ce^{3+}. Further Liu et al. also explained the role of Cl^- for the protection or stabilization of nanorods during the synthesis, whereas NO_3^- may form nanorods although with the time nanorods gets oxidized into nanotubes [25,26]. However, these findings may not be generalized for all synthesis methods.

As mentioned above, nucleation growth from a base and Ce^{3+} salts forms $Ce(OH)_3$ nuclei, which undergo a dissolution and recrystallization process at constant temperature. These $Ce(OH)_3$ nuclei get converted into CeNRs by the Ostwald ripening mechanism. Ji et al. investigated the detailed mechanism of nanorod growth by HRTEM analysis [28]. Oriented attachment and Ostwald ripening were reported as the main growth mechanisms of CeNRs and nanocubes via wet chemical routes. The formation of {111} plane exposed nanorods happens via the attachment of {200} planes of small nuclei while exposing {111} planes predominantly along the {211} plane [25–28]. In this work, we investigated how ceria precursors influenced the morphology and surface defects (Ce^{3+}/ Ce^{4+}) in three types of ceria materials. Specifically, we used $CeCl_3$ precursor for CeNR-1, $CeNO_3$ for CeNR-2, and a calcined $CeCl_3$ originated sample as CeNPs, also described in the synthesis procedure. To study the morphology and physicochemical properties, we employed various techniques. Fig. S2 depicts the XRD patterns of $Ce(OH)_3$ intermediate and Fig. S3 depicts the XRD patterns for the three synthesized samples. Notably, the original indexed {111}, {200}, {220}, {311}, {222}, {400}, {331} and {420} planes are the same as those of a pure fluorite cubic structure (space group Fm3m, JCPDS 01–075-0120) [28–33]. Furthermore, the morphology of all the materials are analysed by TEM. The morphology of the $Ce(OH)_3$ intermediates is illustrated in Fig. S4 (A&B). This figure provides detailed visual information on the structural characteristics of the $Ce(OH)_3$ intermediates. Upon aging, $Ce(OH)_3$ can undergo changes leading to seed nanorods figure S4 (C), including the formation of an intermediate phase before potentially transforming into cerium oxide (CeO_2). The TEM images in Fig. 1 for all three analyzed materials show more and darker pits on CeNR-1 compared to CeNR-2, suggesting the surfaces formed denser and rougher with more (Ce^{3+}/ Ce^{4+}) species. This is consistent with the observations by Liu and coworkers, who found that a higher concentration of defects (Ce^{3+}/ Ce^{4+}) and stronger nanorods observed when $CeCl_3$ was used as a precursor [26]. Moreover, it can also be observed that chloride precursors protect and help to reconstruct CeNRs more effectively compared to nitro precursors. The CeNR-1 derived from chloride precursor's exhibits greater strength, while those from nitro precursors do not demonstrate similar robustness which is visible from the finer nanorods in CeNR-2. The red circle shown in Fig. 1 is likely due to the unreacted cerium hydroxides in CeNR-2. Whereas, CeNPs shows a complete transformation of the nanorod morphology into nanoparticles upon calcination. The obtained BET surface area is shown in table S2 and confirms that in the uncalcined state, the chloride based precursor CeNR-1 yields high surface area than both CeNR-2 and CeNPs. The CeNR-1 sample exhibits abundant oxygen vacancies due to an increased number of surface Ce^{3+} species [34].

Fig. 2(A) shows the temperature-programmed reduction (TPR)

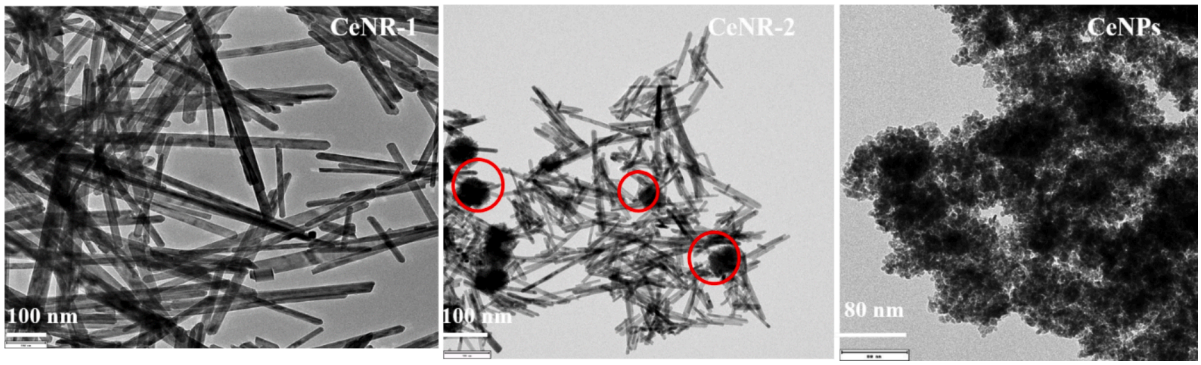

Fig. 1. TEM images of CeNR-1, CeNR-2, and CeNPs.

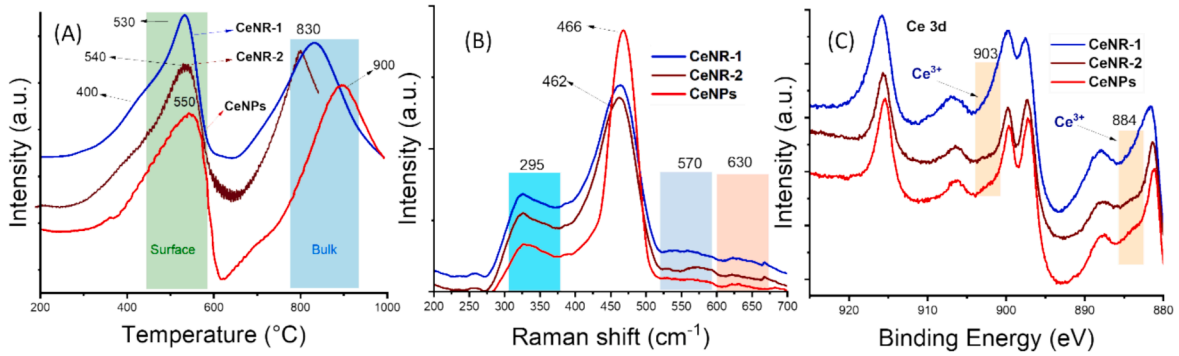

Fig. 2. (A) H_2-TPR profile, (B) Raman analysis, (C) XPS analysis of CeNR-1, CeNR-2, and CeNPs.

profiles for all three materials, revealing two reduction peaks. As it can be seen the low temperature reduction peaks, corresponding to the surface oxygen of CeNR-1, CeNR-2 and CeNPs, lie in the range of 400 °C to 600 °C. In contrast, the reduction peaks for bulk occur at much higher temperatures, from 700 °C to 900 °C. From Fig. 2(A), it is evident that after calcination (CeNPs), the reduction peaks shift to higher temperatures. Judging from the peak shift and area, it is evident that quantitively, for CeNR-1, more ceria is getting reduced in the low temperature peak compared to the second high temperature peak, indicating that the reducibility of this material is higher at lower temperatures. CeNR-2 shows a comparable peak area between first and second peaks, whereas for the calcined CeNPs sample, the reduction trend is reversed, where less amount of ceria is reduced at lower temperatures.

The TPR data were used to set the maximum operating temperature of 700 °C for TCWS to realise the superior redox activity of nanorods over commercial CeO_2 [30–45]. Fig. 2(B) shows the Raman spectra of the synthesized calcined and uncalcined ceria materials, revealing information about their structural defects. All samples exhibit a strong band in the range of 460–468 cm^{-1}, corresponding to F_2g mode vibration of fluorite CeO_2. The weak bands at 280–300 cm^{-1} and 550–650 cm^{-1} are second-order transverse acoustic 2TA mode, the defect-induced mode (D), and the second-order longitudinal optical mode (2LO), respectively [24,34,45,46]. The size-dependent phenomenon in ceria based nanoparticles arises from inhomogeneous strain broadening. This means that variations in particle size cause uneven strain, and the restriction of atomic vibrations (phonons) within the nanoparticles further affects their properties. These two factors together explain the changes in characteristics with nanoparticle size [45,46]. Interestingly, the F_2g peak position for CeNR-1 and CeNR-2 lies around 462 cm^{-1}, with no significant difference observed. Whereas a blue shift was observed for calcined sample CeNPs likely due to the presence of nano cubes as confirmed by TEM analysis. Interestingly, the CeNR-1 peaks at 462 $cm^{-1}$and 570 $cm^{-1}$are slightly broader compared to CeNR-2 and CeNPs [32]. This broader peak shape might indicate the presence of overlapping peaks due to variations in the CeNR-1 structure/morphology or a higher concentration of surface imperfections and defects.

Fig. 2(C) compares the Ce^{3+} and Ce^{4+} oxidation states for the given three samples CeNR-1, CeNR-2, and CeNPs. It can be seen that the Ce^{3+} state is primarily observed overlapping with Ce^{4+} in the 881–883 eV and 901–905 eV regions of all CeNRs. From this comparison, it is evident that CeNR-1 exhibits a higher proportion of Ce^{3+} compared to CeNR-2 and CeNPs. The comparison of three ceria materials oxidation state Ce^{3+} by deconvolution of the XPS spectra is illustrated in Fig. S6. In Fig. S7, the composition of both cerium (Ce) and oxygen (O) in CeNR-1 is shown. Two multiplets were observed in the Ce 3d spectra, corresponding to the spin–orbit coupling of $3d_{5/2}$ and $3d_{3/2}$. Six distinct peaks were identified at 916 eV, 907 eV, 900 eV, 898 eV, 888 eV, and 888.2 eV, corresponding to the binding energies of Ce^{4+} 3d orbitals. Notably, although ceria is primarily composed of Ce^{4+}, a small percentage of Ce^{3+} oxide was detected. This is evident from the presence of peaks at 903 eV and 884 eV, corresponding to the Ce $3d_{3/2}$ and Ce $3d_{5/2}$ components of Ce^{3+} respectively. The analysis reveals that CeO_2 predominantly exists in the Ce^{4+} stable valence state with a minor fraction existing as Ce^{3+} (25 % Ce^{3+} and 75 % Ce^{4+}) [46]. The presence of both Ce^{3+} and Ce^{4+} states suggests a dynamic interplay of redox reactions, contributing to the observed TCWS performance of CeNR-1. The O 1 s peak is at 529 ± 1 eV corresponds to lattice oxygen in ceria, whereas the peak at 532 ± 1 eV maybe attributed to O_2 or CO_2 species [18,19,40–42,21–23,35–39]. A comprehensive analysis utilizing H_2-TPR, Raman spectroscopy, and X-ray Photoelectron Spectroscopy reveals that CeNR-1 exhibits a higher ratio of surface defects [32]. XPS and Raman studies provide important insights into why the calcination process is not favorable for ceria nanorods in water splitting applications. These studies show that calcination not only changes the nanorods' morphology but also affects their crystallographic planes, particularly the (1 1 0) and (1 0 0) surfaces. Such changes can reduce the number of oxygen vacancies, as a result, the calcination process may diminish the overall activity of ceria nanorods in hydrogen production [32–35].

TEM analysis further confirms that CeNR-1 has more robust nanorods, enhancing its stability. The redox cycle of ceria in TCWS involves thermal reduction at high temperatures, as reported by Roeb and Sattler [9]. However, subsequent water oxidation proceeds efficiently at much lower temperatures. This inherent difference necessitates a two-step process with a significant temperature swing for efficient operation [40–48]. The performance of prepared samples for TCWS was evaluated in a fixed bed continuous flow mode. A detailed description of the experimental setup Fig. S1 and operational conditions are provided in the supporting information on pages S2 and S3. The TCWS performance of the prepared samples was also compared with commercial CeNPs. For the commercial sample testing, conventional temperature swing approach was followed where the reduction temperature were varied between were 1000 °C, 1100 °C, and 1200 °C, while the oxidation temperature was kept constant at 900 °C (NTP conditions). This was due to the fact that commercial ceria is completely inactive at lower temperatures. This could also be seen from Fig. S9 that very low hydrogen yield was obtained when reduction was performed at 1000 °C, whereas it reached maximum of ~1.3 mL/g of the material at highest reduction temperature of 1200 °C. Cycling can limit the material lifetime, which can be costly, as noted by Muhich et al. This impact on the material durability can lead to increased operational expenses [10]. Bhosale et al. [48] and Chueh and Haile [50] reported a realistic reduction temperature of 1500 °C and an oxidation temperature of 800 °C, achieving a hydrogen yield exceeding 4.6 mL/g.

The temperature for commercial ceria is three times higher than CeNRs operational temperature under isothermal conditions. The observed yield of hydrogen and the isothermal operation of the cycles are strikingly different when compared to previously reported TCWS cycles [26]. The hydrogen yield was calculated from water cycle phase as described in supporting information page S3-S4. Before starting the isothermal TCWS experiments at 400 °C, we conducted preliminary blank experiments to establish baseline conditions. In the first experiment, the reaction was performed without any ceria material at 400 °C for 90 min cycles, with a water flow rate of 0.01 mL/min and an argon flow rate of 17 mL/min. Under these conditions, no hydrogen production was observed. In the second experiment, the reaction was carried out in the presence of a (CeNR-1) but without water, maintaining an argon flow rate of 17 mL/min. In this case, a trace amount of hydrogen was detected (<0.2 mL/g), indicating minimal activity in the absence of water. These findings highlight the critical role of both the ceria material and water in achieving significant hydrogen production. CeNR-1 was chosen for the blank test because it exhibited the highest hydrogen production under optimized conditions. However, the blank test also confirmed that the uncalcined CeNR-1 showed minimal hydrogen production.

As mentioned above, since the CeNRs in this case were not calcined, surface hydroxides—likely in the form of $Ce(OH)_3$—remain present. Upon heating, these hydroxides begin to decompose > 300 °C, leading to trace amount of hydrogen production. During initial the first 90 min of the reduction phase at 400 °C, all the surface hydroxides decompose, releasing hydrogen. This is followed by an oxidation phase using water/argon 90 min, which yields a significant amount of hydrogen. The effect of temperature on hydrogen yield under isothermal conditions of oxidation and reduction cycles using CeNR-1 is summarized in Fig. 3(A). CeNR-1 exhibited a notable hydrogen production rate of 5.5 mL/g at isothermal temperature of 500 °C. It can be seen that the total hydrogen yield increases with increasing temperature however a sharp decrease is observed after 600 °C and 700 °C. At temperatures above 400 °C, nearly all the hydrogen was produced in the first cycle, suggesting that the nanorods underwent significant sintering after the first cycle, which affected performance in subsequent cycles. This suggests that while reaction kinetics might favour higher temperatures, the material undergoes sintering in starting 90 min of reduction, limiting its ability to produce hydrogen effectively in redox cycles. Owing to this observation and to prevent the material sintering we choose 400 °C as the operating temperature for all three samples as shown in Fig. 3 (B). The CeNR-1 gives highest total hydrogen production (4.7 mL/g) whereas CeNR-2 exhibited a significantly lower hydrogen production rate of 1.5 mL/g, attributed to less denser nanorods and possibly less surface defects (Ce^{3+}/ Ce^{4+}). Calcination of CeNR-1 (resulting in CeNPs) significantly reduced its surface defects (Ce^{3+}/Ce^{4+}) as confirmed by X-ray Photoelectron Spectroscopy (XPS), explaining its inability to produce hydrogen compared to the CeNR-1. This highlights the importance of surface defects for CeNRs functionality, as they act as active sites for water oxidation and hydrogen production. As can be seen, CeNR-1 exhibits a significantly higher hydrogen production in the three different cycles Fig. 3C. In first cycle CeNR-1 shows more hydrogen production, this initial boost in hydrogen yield is due to the presence of extra oxygen vacancies in the material, which were introduced during the synthesis process. This has been confirmed by Raman spectroscopy and XPS analysis. CeNR-2 exhibited lower hydrogen production compared to the CeNR-1. Despite the favourable reaction kinetics at 400 °C, it was found that the material suffered from sintering after the first cycle and decreases its surface defects as it can be seen in TEM analysis in Fig. S5 as well as XPS of the spent sample in Fig. S8. The material obtained after the initial cycles may have undergone significant structural reconstruction as a result of temperature and water oxidation. This reconstruction likely altered the material properties, necessitating higher temperatures for subsequent cycles and various metal doping studies to achieve the desired performance and stability. We believe that this work forms a solid foundation for future directions, including doping CeNRs

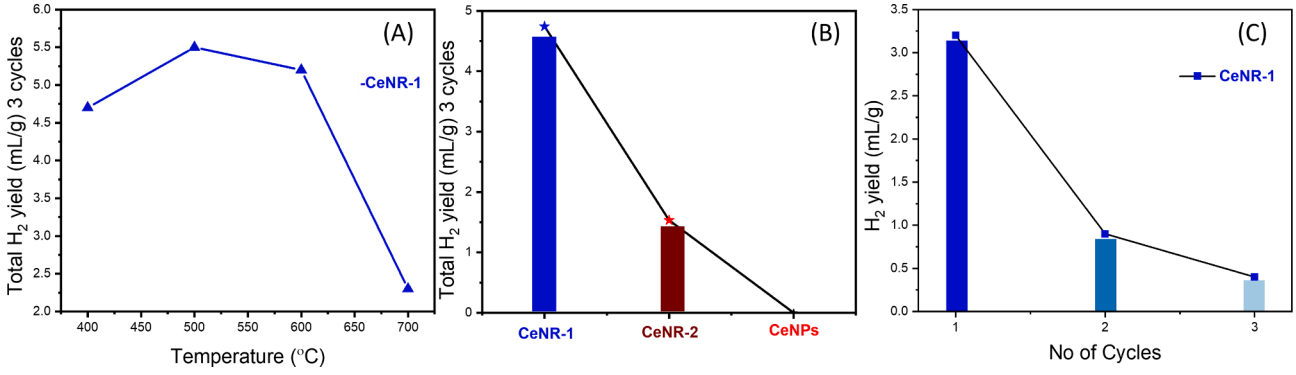

Fig. 3. (A)Total hydrogen yield in three redox cycles at different temperatures for CeNR-1 (H_2O flow 0.01 mL/min, Reduction phase-Argon 90 min and oxidation Argon/H_2O 90 min, amount of CeNR-1 is 0.2 g), (B) Total hydrogen yield in three redox cycles for different material at 400 °C (H_2O flow 0.01 mL/min, Reduction phase-Argon 90 min and oxidation Argon/H_2O 90 min, material amount is 0.2 g), (C) Per redox cycle hydrogen yield for at 400 °C for CeNR-1.

with transition metals (e.g., Fe, Pt, Zr) to enhance stability, optimizing synthesis methods to reduce sintering, and refining reactor conditions to improve material stability.

3. Conclusion

In summary, it was observed that CeNRs with higher surface defects (Ce^{3+}/Ce^{4+}) have great potential as a redox material for Thermochemical Water Splitting (TCWS). CeNR-1, exhibiting a higher Ce^{3+} concentration, demonstrated superior hydrogen production (4.7 mL/g) at a significantly lower temperature (400 °C) than CeNR-2 and CeNPs. XPS and Raman spectroscopy confirmed the role of Ce^{3+} in enhancing TCWS performance. However, calcination at 500 °C altered CeNR-1′s morphology, increasing Ce^{4+} content and lowering hydrogen production. TEM analysis revealed sintering at 400 °C after the first redox cycle, highlighting the need for further studies on dopant modifications to improve stability and efficiency. These findings mark a significant step in lowering TCWS operation temperatures. We believe that these findings have potential impact in accelerating the research in the TCWS route.

CRediT authorship contribution statement

Dhanaji R.Naikwadi: Writing – review & editing, Writing – original draft, Visualization, Methodology, Investigation, Formal analysis, Data curation. **Vaishnavi Ganesh:** Validation, Methodology, Investigation, Data curation. **Hesham Sharaf:** Validation, Methodology, Investigation, Formal analysis, Data curation. **Michele Offidani:** Validation, Methodology, Investigation. **Stefania Albonetti:** Writing – review & editing, Supervision, Funding acquisition, Conceptualization. **Nikolaos Dimitratos:** Writing – review & editing, Supervision, Resources, Formal analysis, Conceptualization. **Atul Bansode:** Writing – review & editing, Validation, Resources, Project administration, Methodology, Investigation, Funding acquisition, Formal analysis, Data curation, Conceptualization.

Declaration of competing interest

The authors declare the following financial interests/personal relationships which may be considered as potential competing interests: [Atul Bansode, Vaishnavi Ganesh, Michele Offidani have a patent application (NL2034721) titled Low temperature thermochemical water splitting in the Netherlands . If there are other authors, they declare that they have no known competing financial interests or personal relationships that could have appeared to influence the work reported in this paper].

Appendix A. Supplementary data

Supplementary data to this article can be found online at https://doi.org/10.1016/j.fuel.2025.135251.

Data availability

Data will be made available on request.

References

[1] Goelzer H, Nowicki S, Payne A, Larour E, Seroussi H, Lipscomb WH. The future sea-level contribution of the Greenland ice sheet: a multi-model ensemble study of ISMIP6. Cryosphere 2020;14:3071–96. https://doi.org/10.5194/tc-14-3071-2020.

[2] Li B, Development of Active and Stable Nanostructured Ceria-based Catalysts for Soot Oxidation. 2019.

[3] Gogoi P, Tudu B, Saikia P. Hydrogen Fuel: Clean Energy Production Technologies 2022:133–54. doi: 10.1007/978-981-16-4505-1_7.

[4] Nnabuife SG, Ugbeh-Johnson J, Okeke NE, Ogbonnaya C. Present and projected developments in hydrogen production: a technological review. Carbon Capture Sci Technol 2022:3. https://doi.org/10.1016/j.ccst.2022.100042.

[5] Li M, Verkuil J, Bunea S, Kortlever R, Urakawa A. Towards higher NH_3 faradaic efficiency: selective-poisoning of HER active sites by Co-feeding CO in NOElectroreduction. ChemSusChem 2023;16:1–5. https://doi.org/10.1002/cssc.202300949.

[6] Lee JE, Shafiq I, Hussain M, Lam SS, Rhee GH, Park YK. A review on integrated thermochemical hydrogen production from water. Int J Hydrogen Energy 2022;47:4346–56. https://doi.org/10.1016/j.ijhydene.2021.11.065.

[7] Singh R, Dutta S. A review on H_2 production through photocatalytic reactions using TiO_2/TiO_2-assisted catalysts. Fuel 2018;220:607–20. https://doi.org/10.1016/j.fuel.2018.02.068.

[8] Canan A, Dincer I. Comparative assessment of hydrogen production methods from renewable and non-renewable sources. Int J Hydrogen Energy 2014;39:1–2. https://doi.org/10.1016/j.ijhydene.2013.10.060.

[9] Roeb M, Sattler C. Isothermal water splitting. Science (80-) 2013;341:470–1. https://doi.org/10.1126/science:124131.

[10] Martinek J, Musgrave CB, Weimer AW, Muhich CL, Evanko BW, Weston KC, et al. Efficient Generation of H_2 by Splitting Water with an Isothermal Redox Cycle. Science (80-) 2013;341:540–3. https://doi.org/10.1126/science:1239454.

[11] Liao Y, He L, Zhao M, Ye D. Ultrasonic-assisted hydrothermal synthesis of ceria nanorods and their catalytic properties for toluene oxidation. J Environ Chem Eng 2017;5:5054–60. https://doi.org/10.1016/j.jece:2017.09.037.

[12] Mao Y, Gao Y, Dong W, Wu H, Song Z, Zhao X, et al. Hydrogen production via a two-step water splitting thermochemical cycle based on metal oxide – a review. Appl Energy 2020:267. https://doi.org/10.1016/j.apenergy.2020.114860.

[13] Han SB, Kang TB, Joo OS, Jung KD. Water splitting for hydrogen production with ferrites. Sol Energy 2007;81:623–8. https://doi.org/10.1016/j.solener.2006.08.012.

[14] Krishnan A, Sreeremya TS, Murray E, Ghosh S. One-pot synthesis of ultra-small cerium oxide nanodots exhibiting multi-colored fluorescence. J Colloid Interface Sci 2013;389:16–22. https://doi.org/10.1016/j.jcis.2012.09.009.

[15] Pan C, Zhang D, Shi L, Fang J. Template-free synthesis, controlled conversion, and CO oxidation properties of CeO_2 nanorods, nanotubes, nanowires, and nanocubes. Eur J Inorg Chem 2008:2429–36. https://doi.org/10.1002/ejic.200800047.

[16] Sun C, Li H, Chen L. Nanostructured ceria-based materials: synthesis, properties, and applications. Energ Environ Sci 2012;5:8475–505. https://doi.org/10.1039/c2ee22310d.

[17] Zhou K, Wang X, Sun X, Peng Q, Li Y. Enhanced catalytic activity of ceria nanorods from well-defined reactive crystal planes. J Catal 2005;229:206–12. https://doi.org/10.1016/j.jcat.2004.11.004.

[18] Bhosale RR. Solar hydrogen production via thermochemical magnesium oxide – Magnesium sulfate water splitting cycle. Fuel 2020:275. https://doi.org/10.1016/j.fuel.2020.117892.

[19] Meredig B, Wolverton C. First-principles thermodynamic framework for the evaluation of thermochemical H_2O - Or CO_2 -splitting materials. Phys Rev B - Condens Matter Mater Phys 2009:80. https://doi.org/10.1103/PhysRevB.80.245119.

[20] Kodama T. High-temperature solar chemistry for converting solar heat to chemical fuels. Prog Energy Combust Sci 2003;29:567–97. https://doi.org/10.1016/S0360-1285(03)00059-5.

[21] Abanades S. Metal oxides applied to thermochemical water-splitting for hydrogen production using concentrated solar energy. ChemEngineering 2019;3:1–28. https://doi.org/10.3390/chemengineering3030063.

[22] He H, Yang P, Li J, Shi R, Chen L, Zhang A, et al. Controllable synthesis, characterization, and CO oxidation Activityof CeO_2 nanostructures with various morphologies. Ceram Int 2016;42(6):7810–8. https://doi.org/10.1016/j.ceramint.2016.02.005.

[23] Abanades S, Legal A, Cordier A, Peraudeau G, Flamant G, Julbe A. Investigation of reactive cerium-based oxides for H_2 production by thermochemical two-step water-splitting. J Mater Sci 2010;45:4163–73. https://doi.org/10.1007/s10853-010-4506-4.

[24] Lin J, Li L, Huang Y, Zhang W, Wang X, Wang A, et al. In situ calorimetric study: structural effects on adsorption and catalytic performances for CO oxidation over Ir-in-CeO_2 and Ir-on-CeO_2 catalysts. J Phys Chem C 2011;115:16509–17. https://doi.org/10.1021/jp204288h.

[25] Wu T, Cui J, Wang C, Zhang G, Li L, Qu Y, et al. Oxygen vacancy-mediated activates oxygen to produce Reactive Oxygen Species (ROS) on Ce-Modified activated clay for degradation of organic compounds without hydrogen peroxide in strong acid. Nanomaterials 2022;12. https://doi.org/10.3390/nano12244410.

[26] Liu X, Zhou K, Wang L, Wang B, Li Y. Oxygen vacancy clusters promoting reducibility and activity of ceria nanorods. J Am Chem Soc 2009;131:3140–1. https://doi.org/10.1021/ja808433d.

[27] Agarwal S, Zhu X, Hensen EJM, Lefferts L, Mojet BL. Defect chemistry of ceria nanorods. J Phys Chem C 2014;118:4131–42. https://doi.org/10.1021/jp409989y.

[28] Ji Z, Wang X, Zhang H, Lin S, Meng H, Sun B. Designed synthesis of CeO_2 nanorods and nanowires for studying toxicological effects of high aspect ratio nanomaterials. ACS Nano 2012;6:5366–80. https://doi.org/10.1021/nn3012114.

[29] Wu Q, Zhang F, Xiao P, Tao H, Wang X, Hu Z, Lu Y. Great influence of anions for controllable synthesis of CeO_2 nanostructures: from nanorods to nanocubes. J. Phys. Chem. C 2008;112(44):17076–80. https://doi.org/10.1021/jp805753b.

[30] Oudejans D, Offidani M, Constantinou A, Albonetti S, Dimitratos N, Bansode A. Comprehensive review on Two-Step thermochemical water splitting for hydrogen production in a redox cycle. Energies 2022;15. https://doi.org/10.3390/en15093044.

[31] Kim NW, Lee DK, Yu H. Selective shape control of cerium oxide nanocrystals for photocatalytic and chemical sensing effect. RSC Adv 2019;9:13829–37. https://doi.org/10.1039/c9ra01519a.

[32] Loridant S. Raman spectroscopy as a powerful tool to characterize ceria-based catalysts. Catal Today 2021;373:98–111. https://doi.org/10.1016/j.cattod.2020.03.044.
[33] Agarwal S, Lefferts L, Mojet BL. Ceria nanocatalysts: shape dependent reactivity and formation of OH. ChemCatChem 2013;5:479–89. https://doi.org/10.1002/cctc.201200491.
[34] Wang L, Yu Y, He H, Yan Z, Xiubo Q, Baoyi W. Oxygen vacancy clusters essential for the catalytic activity of CeO_2 nanocubes for o-xylene oxidation. Sci Rep 2017:12845. https://doi.org/10.1038/s41598-017-13178-6.
[35] Ganzoury MA, Fateen SEK, El Sheltawy ST, Radwan AM, Allam NK. Thermodynamic and efficiency analysis of solar thermochemical water splitting using Ce-Zr mixtures. Sol Energy 2016;135:154–62. https://doi.org/10.1016/j.solener.2016.05.053.
[36] Orfila M, Sanz D, Linares M, Molina R, Sanz R, Marugán J, et al. H_2 production by thermochemical water splitting with reticulated porous structures of ceria-based mixed oxide materials. Int J Hydrogen Energy 2021;46:17458–71. https://doi.org/10.1016/j.ijhydene.2020.04.222.
[37] Kaneko H, Miura T, Ishihara H, Taku S, Yokoyama T, Nakajima H, et al. Reactive ceramics of CeO_2-MOx (M=Mn, Fe, Ni, Cu) for H_2 generation by two-step water splitting using concentrated solar thermal energy. Energy 2007;32:656–63. https://doi.org/10.1016/j.energy.2006.05.002.
[38] Gokon N, Suda T, Kodama T. Thermochemical reactivity of 5–15 mol% Fe Co, Ni, Mn-doped cerium oxides in two-step water-splitting cycle for solar hydrogen production. Thermochim Acta 2015;617:179–90. https://doi.org/10.1016/j.tca.2015.08.036.
[39] Schmitt R, Nenning A, Kraynis O, Korobko R, Frenkel AI, Lubomirsky I, et al. A review of defect structure and chemistry in ceria and its solid solutions. Chem Soc Rev 2020;49:554–92. https://doi.org/10.1039/c9cs00588a.
[40] Schwarz K. Materials design of solid electrolytes. PNAS 2006;103:3497. https://doi.org/10.1073/pnas.0600327103.
[41] Melchionna M, Fornasiero P. The role of ceria-based nanostructured materials in energy applications. Mater Today 2014;17:349–57. https://doi.org/10.1016/j.mattod.2014.05.005.
[42] Jayakumar G, Irudayaraj AA, Raj AD. Particle size effect on the properties of cerium oxide (CeO_2) manoparticles synthesized by hydrothermal method. Mech Mater Sci Eng J 2017;9:2–7. https://doi.org/10.2412/mmse.3.4.481.
[43] do Sacramentoa EM, Salesa AD, de Limaa LC, Nejat Veziroglu T. A solar–wind hydrogen energy system for the Ceará state–Brazil. Int J Hydrogen Energy 2008;33:5304–11. https://doi.org/10.15518/isjaee.2019.07-09.032-042.
[44] Gallucci F, Fernandez E, Corengia M, van Sint Annaland P, Chem. Eng. Sci, Recent advances on membranes and membrane reactors for hydrogen production 2013;92:40-66.doi: 10.1016/j.ces.2013.01.008.
[45] Zili Wu, Li M, Howe J, Meyer HM, Overbury SH. Probing defect sites on CeO_2 nanocrystals with well-defined surface planes by raman spectroscopy and O_2 adsorption. Langmuir 2010;26:16595–606. https://doi.org/10.1021/la101723w.
[46] Spanier JE, Robinson RD, Zheng F, Chan SW, Herman IP. Size-dependent properties of CeO_2 -y nanoparticles as studied by Raman scattering. PhysRevB 2001;64(24). https://doi.org/10.1103/PhysRevB.64.245407.
[47] Tofighi A, Sibieude F. Dissociation of magnetite in a solar furnace for hydrogen production. Tentative production evaluation of a 1000 kW concentrator from small scale (2 kW) experimental results. Int J Hydrogen Energy 1984;9:293. https://doi.org/10.1016/0360-3199(84)90079-X.
[48] Bhosale RR, Takalkar G, Sutar P, Kumar A, AlMomani F, Khraisheh M. A decade of ceria based solar thermochemical H_2O/CO_2 splitting cycle. Int J Hydrogen Energy 2019;44:34e60. https://doi.org/10.1016/j.ijhydene.2018.04.080.
[49] Maria U, Alzueta V, Mercader A, Cuoci S, Gersen H, Glarborg HP. Flow reactor oxidation of Ammonia-Hydrogen fuel mixtures. Energy Fuel 2024;38:3369–81. https://doi.org/10.1021/acs.energyfuels.3c03929.
[50] Chueh WC, Haile SM. Ceria as a thermochemical reaction medium for selectively generating syngas or methane from H_2O and CO_2. ChemSusChem 2009;2:735–9. https://doi.org/10.1002/cssc.200900138.
[51] Roychowdhury S, Mukthar AM, Dhua S, Sundararajan T, Ranga RG. Thermochemical hydrogen production using $Rh/CeO_2/\gamma$-Al_2O_3 catalyst by steam reforming of ethanol and water splitting in a packed bed reactor. Int J Hydrogen Energy 2021;46:19254–69. https://doi.org/10.1016/j.ijhydene.2021.03.079.
[52] Seo K, Lim T, Mills EM, Kim S, Ju S. Hydrogen generation enhanced by nano-forest structures. RSC Adv 2016;6:12953–8. https://doi.org/10.1039/C5RA26226G.
[53] Costa OFA, Barreiros MA, Haeussler A, Caetano APF, Mouquinho AI, Oliveira e Silva PM, et al. High performance cork-templated ceria for solar thermochemical hydrogen production via two-step water-splitting cycles. Sustainable Energy Fuels 2020;4(6):3077–89. https://doi.org/10.1039/D0SE00318B.
[54] Kodama T, Gokon N, Yamamoto R. Thermochemical two-step water splitting by ZrO_2-supported $NixFe_3{-}xO_4$ for solar hydrogen production. Sol Energy 2008;82:73–9. https://doi.org/10.1016/j.solener.2007.03.005.
[55] Kodama T, Nakamuro Y, Mizuno TA. Two-Step thermochemical water splitting by iron-oxide on stabilized zirconia. J Sol Energy Eng 2004;128:3–7. https://doi.org/10.1115/1.1878852.
[56] Fresno F, Fernández-Saavedra R, Belén Gómez-Mancebo M, Vidal A, Sánchez M, Isabel Rucandio M, et al. Solar hydrogen production by two-step thermochemical cycles: evaluation of the activity of commercial ferrites. Int J Hydrogen Energy 2009;34:2918–24. https://doi.org/10.1016/j.ijhydene.2009.02.020.
[57] Amar V, Puszynski J, Shende R. H_2 generation from thermochemical water-splitting using yttria stabilized NiFe2O4 core-shell nanoparticles. J Renew Sustain Energy 2015;7:023113.
[58] Chueh WC, Falter C, Abbott M, Scipio D, Furler P, Haile SM, et al. High-flux solar-driven thermochemical dissociation of CO_2 and H_2O using nonstoichiometric ceria. Science (New York, NY) 2010;330:1797e801. doi:10.1126/science:1197834.
[59] Melchionna M, Fornasiero P. The role of ceria-based nanostructured materials in energy applications. Mater Today 2014;17:349e57. https://doi.org/10.1016/j.mattod.2014.05.005.
[60] Kaneko H, Ishihara H, Taku S, Naganuma Y, Hasegawa N, Tamaura Y. Cerium ion redox system in CeO_2-xFe_2O_3 solid solution at high temperatures (1,273–1,673 K) in the two-step water-splitting reaction for solar H2 generation. J Mater Sci 2008;43:3153e61. https://doi.org/10.1007/s10853-008-2499-z.
[61] Charvin P, Abanades S, Beche E, Lemont F, Flamant G. Hydrogen production from mixed cerium oxides via threestep water-splitting cycles. Solid State Ion 2009;180:1003e10. https://doi.org/10.1016/j.ssi.2009.03.015.